The Astrophysical Journal, 773:122 (6pp), 2013 August 20 doi:10.1088/0004-637X/773/2/122

THE OPTICAL COUNTERPART TO THE X-RAY TRANSIENT IGR J1824−24525 IN THE GLOBULAR CLUSTER M28*

C. Pallanca[1], E. Dalessandro[1], F. R. Ferraro[1], B. Lanzoni[1], and G. Beccari[2]
[1] Dipartimento di Fisica e Astronomia, Università degli Studi di Bologna, Viale Berti Pichat 6/2, I-40127 Bologna, Italy; cristina.pallanca3@unibo.it
[2] European Southern Observatory, Karl-Schwarzschild-Strasse 2, D-85748 Garching bei München, Germany
Received 2013 May 10; accepted 2013 June 21; published 2013 August 1

ABSTRACT

We report on the identification of the optical counterpart to the recently detected *INTEGRAL* transient IGR J1824−24525 in the Galactic globular cluster M28. From analysis of a multi-epoch *Hubble Space Telescope* data set, we have identified a strongly variable star positionally coincident with the radio and *Chandra* X-ray sources associated with the *INTEGRAL* transient. The star has been detected during both a quiescent and an outburst state. In the former case it appears as a faint, unperturbed main-sequence star, while in the latter state it is about two magnitudes brighter and slightly bluer than main-sequence stars. We also detected Hα excess during the outburst state, suggestive of active accretion processes by the neutron star.

Key words: binaries: close – globular clusters: individual (M28) – stars: neutron – X-rays: individual (IGR J18245-2452)

1. INTRODUCTION

The high stellar densities and the frequent dynamical interactions occurring in globular cluster (GC) cores are expected to significantly affect the formation and the evolution of exotic populations such as low-mass X-ray binaries (LMXBs), cataclysmic variables, millisecond pulsars (MSPs), and blue straggler stars (e.g., Bailyn 1995; Verbunt et al. 1997; Grindlay et al. 2001; Pooley et al. 2003; Ferraro et al. 2009). In fact, these objects are thought to result from the evolution of various kinds of binary systems originating from and/or hardened by stellar interactions (e.g., Clark 1975; Hills & Day 1976; Bailyn 1992; Ivanova et al. 2008), and are therefore considered powerful diagnostics of GC dynamical evolution (e.g., Ferraro et al. 1995, 2012; Goodman & Hut 1989; Hut et al. 1992; Meylan & Heggie 1997; Pooley et al. 2003; Fregeau 2008). However, many open questions still remain about their formation and evolutionary paths.

When a close binary system contains a compact object, mass transfer processes can take place. The streaming gas, its impact on the compact star, or the presence of an accretion disk can produce significant X-ray and UV radiation together with emission lines (such as the Hα) or rapid luminosity variations. The first evidence of interacting binaries in Galactic GCs was indeed obtained through the discovery of X-ray sources. In particular, LMXBs are thought to be binary systems with an accreting neutron star (NS) and are characterized by X-ray luminosities larger than $\sim 10^{35}$ erg s^{-1}. Their final stage is thought to be a binary system containing a very fast NS (an MSP), spun up through mass accretion from the evolving companion. Moreover, during their life, some LMXBs, usually called X-ray transients (White et al. 1984), show a few outbursts and, during the quiescent state, their millisecond pulsation can become detectable (Chakrabarty & Morgan 1998).

The identification of optical counterparts is a fundamental step in characterizing exotic binary systems, in both the quiescent and the outburst states, and in clarifying their formation and evolutionary processes (Testa et al. 2012). Determining the nature and the properties of the companion (which dominates the optical emission in the quiescent state) is also very useful to tightly constrain the orbital parameters of the system (e.g., D'Avanzo et al. 2009; Engel et al. 2012). In the case of GCs, it also represents a crucial tool for quantifying the occurrence of dynamical interactions, understanding the effects of crowded stellar environments on the evolution of binaries, and determining the shape of the GC potential well (e.g., Phinney 1992; Bellazzini et al. 1995; Possenti et al. 2003; Ferraro et al. 2003).

M28 (NGC 6626) is a Galactic GC with an intermediate central density ($\log \rho_0 = 4.9$ in units of $M_\odot$ pc^{-3}; Pryor & Meylan 1993) and a relatively high metallicity ([Fe/H] = −1.32; Harris 1996, 2010 version) located at ∼6.8 kpc from Earth in the direction of the Galactic center (Harris 1996). It is the first Galactic GC where an MSP was discovered (Lyne et al. 1987) and it is currently known to host the third largest population of pulsars among all GCs (Bégin 2006; Bogdanov et al. 2011).[3] A total of 46 X-ray sources, of which 12 lie within one core radius ($r_c = 14\farcs4$; Harris 1996) from the center, have been detected with *Chandra* (Becker et al. 2003).

During the observations of the Galactic center performed on 2013 March 28 with the *International Gamma-Ray Astrophysics Laboratory* (*INTEGRAL*), a new hard X-ray transient (IGR J18245−2452) was revealed in the direction of M28 (Eckert et al. 2013). Subsequent observations with *Swift*/XRT confirmed the detection of the transient source and its location within the core of the cluster, at $\alpha_{2000} = 18^{\rm h}24^{\rm m}32\fs20$ and $\delta_{2000} = -24^\circ52'05\farcs5$, with error radius $3\farcs5$ (at 90% confidence; Heinke et al. 2013; Romano et al. 2013). *Swift*/XRT time-resolved spectroscopy performed on 2013 April 7 revealed a thermal spectrum with a "cooling tail," unambiguously identifying the burst as thermonuclear and suggesting that the source is a low-luminosity LMXB in the hard state where an NS is accreting matter from a companion (Linares 2013; see also Serino et al. 2013). A radio follow-up was performed with ATCA on 2013 April 5, for a total of 6 hr, at two different frequencies (9 and 5.5 Hz). A single source was identified

* Based on observations collected with the NASA/ESA *Hubble Space Telescope* (Prop. 19835), obtained at the Space Telescope Science Institute, which is operated by AURA, Inc., under NASA contract NAS5-26555.

[3] For the complete list of pulsars in Galactic GCs unambiguously, see the Web site: http://www.naic.edu/~pfreire/GCpsr.html.

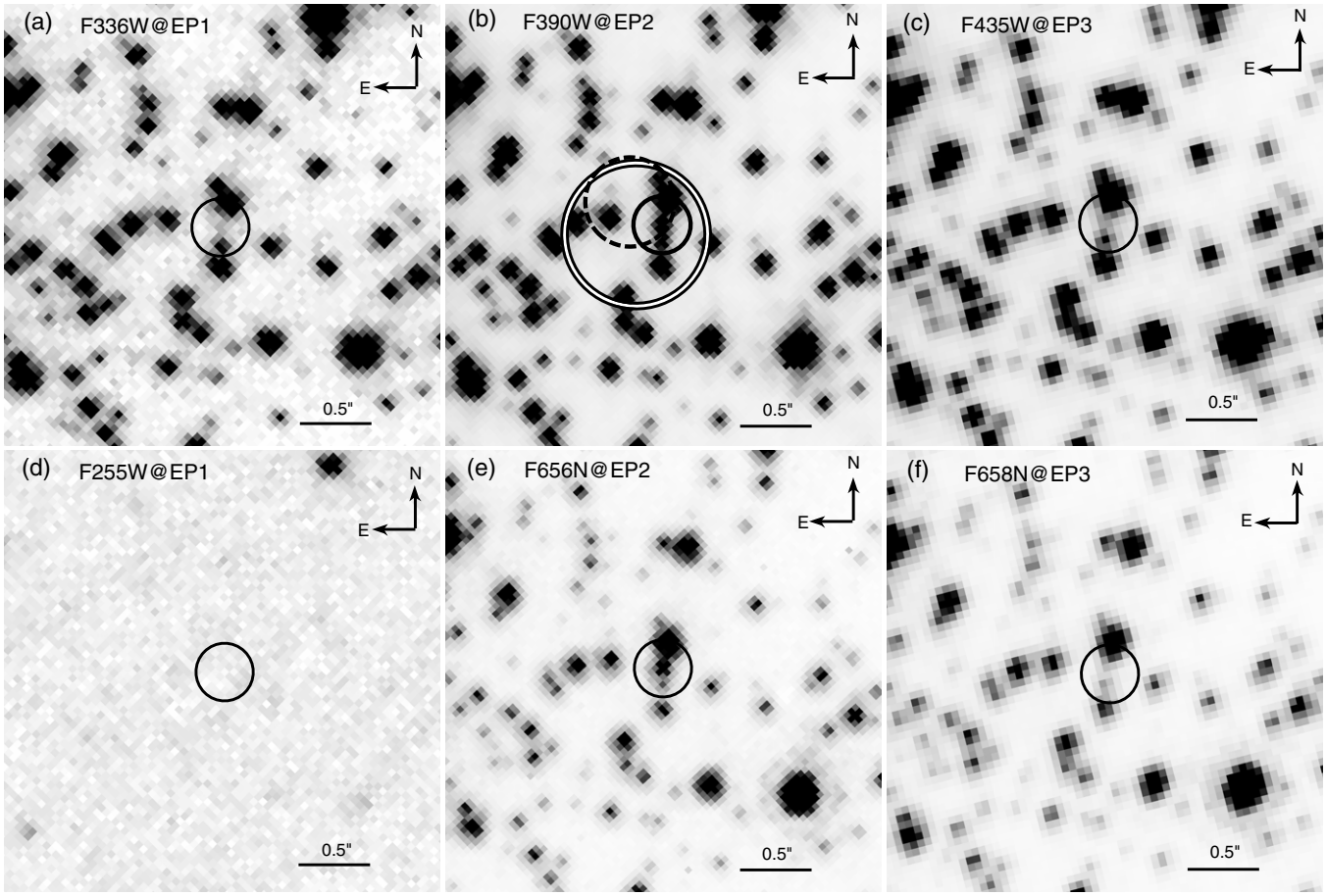

Figure 1. *HST* images of the optical counterpart (solid circle) to IGR J1824−24525. The filters and epochs of observation are labeled in each panel (see Table 1 for more details). Clearly, the source is in a quiescent state in EP1 and EP3 (leftmost and rightmost panels) while it has been caught in the outburst state during EP2 (central panels). In panel (b) the double and dashed circles mark, respectively, the position of the variable ATCA source detected by Pavan et al. (2013) and the *Chandra* X-ray source 23 (Becker et al. 2003), with the radii corresponding to the quoted astrometric uncertainties.

Table 1
Summary of the Multi-epoch Data Sets Used in This Work

Epoch	Date	Instrument	Filter	t_{exp} (s)	State	Proposal ID/PI
EP1	2009 Apr 7	WFPC2/PC	F170W	2 × 1700	Q	GO11975/Ferraro
			F255W	3 × 1200		
			F336W	3 × 800		
			F555W	2 × 80		
EP2	2009 Aug 9	WFC3/UVIS	F390W	5 × 850 + 1 × 800	B	GO11615/Ferraro
			F606W	7 × 200		
			F814W	7 × 200		
			F656N	2 × 1100 + 1 × 1070		
				3 × 1020 + 1 × 935		
EP3	2010 Apr 26	ACS/WFC	F435W	4 × 464	Q	GO11340/Grindlay
			F625W	4 × 60		
			F658N	6 × 724 + 3 × 717		

Note. The quiescent and outburst states (see Section 3) are marked by the letters Q and B, respectively.

at $\alpha_{2000} = 18^h24^m32^s.51$ and $\delta_{2000} = -24°52'07''.9$, with a 90% confidence error of 0″.5 (Pavan et al., 2013). This position is only marginally consistent with that derived from the *Swift*/XRT data, but the detected strong variability (reaching up to 2.5 times the mean flux density during the first 90 minutes of observations) suggests a possible association with the X-ray transient. Its position corresponds well to the location of the X-ray source 23 identified by Becker et al. (2003) from *Chandra* observations and associated with IGR J1824−24525 by Homan & Pooley (2013).

Here we report on the identification of the optical counterpart to IGR J1824−24525, obtained from the analysis of high-resolution *Hubble Space Telescope* (*HST*) data acquired with the Wide Field Planetary Camera 2 (WFPC2), Wide Field Camera 3 (WFC3), and Advanced Camera for Surveys (ACS)/WFC in three different epochs (see also Pallanca et al. 2013, and Cohn

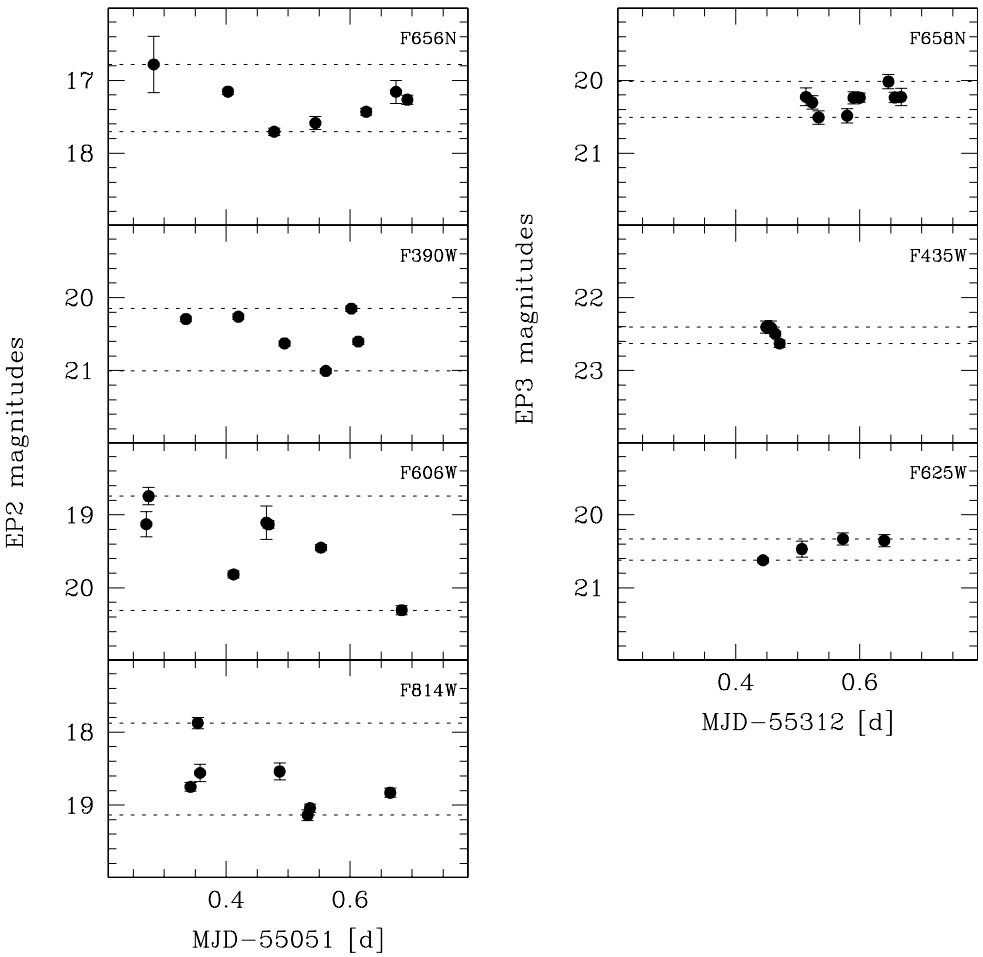

Figure 2. Light curves of the optical counterpart to IGR J1824−24525 during the outburst state (left panels) and the quiescent state (right panels). The dotted lines mark the maximum range of variability detected by each set of observations. Photometric errors are reported, but in most cases are smaller than the point size.

et al. 2013). In Section 2, we describe the data set and the data analysis procedure. The properties of the optical counterpart to IGR J1824−24525 are presented in Section 3 and discussed in Section 4.

2. OBSERVATIONS AND DATA ANALYSIS

For this work we adopted the same catalog used to identify the companion to PSR J1824−2452H and fully described in Pallanca et al. (2010). In order to unveil luminosity variations among different epochs, two additional sets of *HST* data acquired with the WFPC2 and the ACS have been analyzed. In particular, because we were interested only in the GC core, we limited the analysis to the Planetary Camera (PC) of the WFPC2 and CHIP2 of the ACS/WFC mosaic. The available samples have been acquired through various filters, at three different epochs (see Table 1): the WFPC2 data set was collected on 2009 April 7 (epoch 1, hereafter EP1), WFC3 observations were performed on 2009 August 9 (epoch 2, EP2), and the ACS data set was acquired on 2010 April 26 (epoch 3, EP3).

The data reduction procedure for the ACS sample was performed on the CTE-corrected (flc) images, once they were corrected for the pixel area map using standard IRAF procedures. The photometric analysis was carried out using the DAOPHOT package (Stetson 1987). For each image we modeled the point-spread function (PSF) by using a large number (∼100) of bright and nearly isolated stars. Then, all F435W and F625W images were combined with MONTAGE2 and used to produce a master frame on which we optimized a master list of stars. Finally, we performed the PSF fitting on this master list by using the DAOPHOT packages ALLSTAR and ALLFRAME (Stetson 1987, 1994). A similar procedure was adopted to reduce the flat-fielded (c0m) WFPC2 images.

Since the ACS images heavily suffer from geometric distortions within the field of view, we corrected the instrumental positions of stars by applying the equations reported by Sirianni et al. (2005). Through cross-correlation, we then placed the ACS and the WFPC2 data sets on the same astrometric system of the WFC3 sample for which the astrometric solution has an accuracy of ∼0.″2 in both right ascension and declination (Pallanca et al. 2010).

Finally, the instrumental magnitudes were calibrated to the VEGAMAG system by using the photometric zero points reported on the instrument Web site[4] and the procedure described in Holtzman et al. (1995) and Sirianni et al. (2005) for WFPC2 and ACS, respectively.

3. THE OPTICAL COUNTERPART TO IGR J18245−2452

During a systematic study of the GC M28 aimed at searching for the companion stars to binary MSPs, we found a peculiar object (see Figure 1) located at $\alpha_{2000} = 18^{h}24^{m}32^{s}.50$ and

[4] www.stsci.edu/hst/acs/analysis/zeropoints/zpt.py and www.stsci.edu/documents/dhb/web/c32_wfpc2dataanal.fm1.html for ACS and WFPC2, respectively.

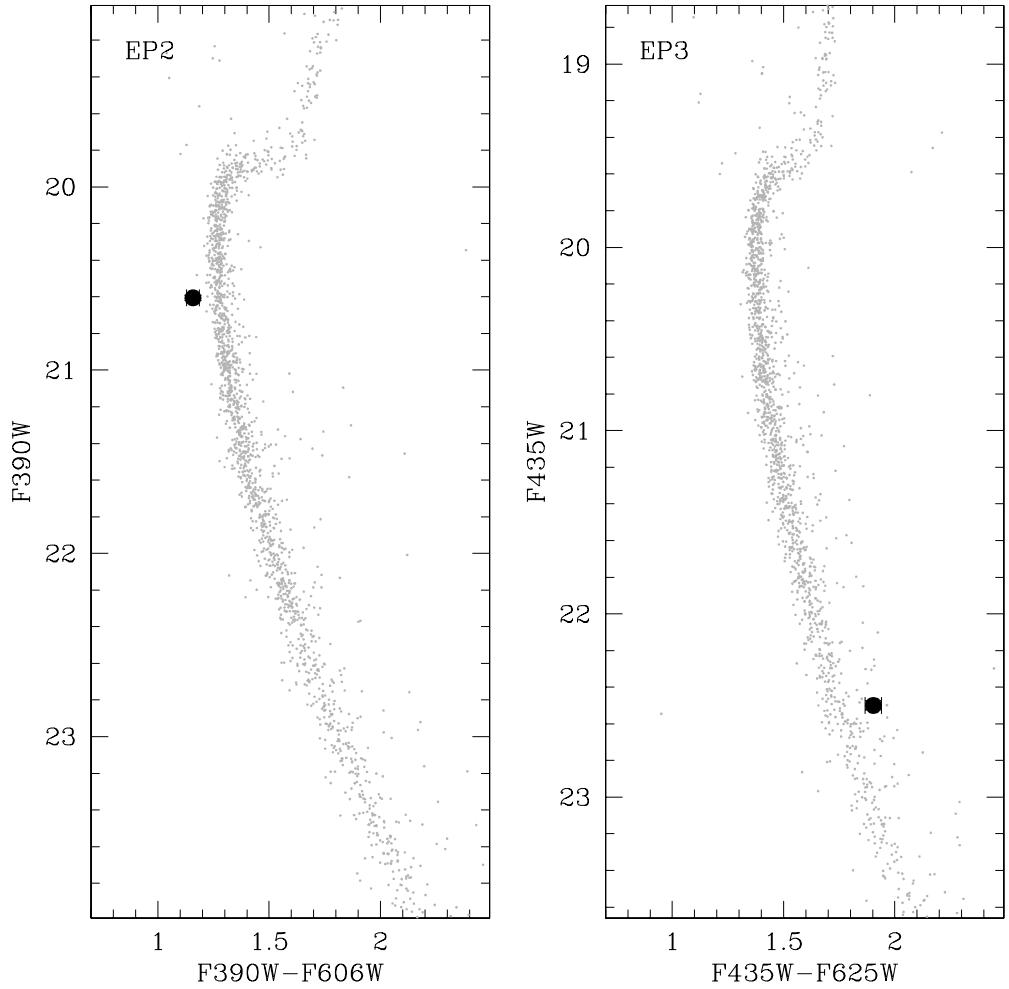

Figure 3. Color–magnitude diagrams obtained during outburst epoch (left panel) and quiescence epoch (right panel) for all stars (gray points) located within 10″ from IGR J1824−24525. The location of the optical counterpart to IGR J1824−24525, as obtained by averaging the observed light curves (see Figure 2 and footnote 3), is shown as a large solid circle.

$\delta_{2000} = -24°52'07''.8$, in very good agreement with the position of the X-ray source 23 reported by Becker et al. (2003) and of the variable ATCA radio source discussed by Pavan et al. (2013).

In EP2 this star showed a strong and irregular variability in each filter on a timescale of ∼10 hr (Figure 2). Based on the mean magnitudes[5] (F390W = 20.61 ± 0.01, F606W = 19.45 ± 0.02, F814W = 18.83 ± 0.03, and F656N = 17.42 ± 0.02), this star turned out to be about 0.5–1 mag fainter than the main-sequence (MS) turnoff (TO) and bluer than the MS both in the (F390W, F390W-F606W) and in the (F606W, F606W-F814W) color–magnitude diagrams (CMDs; see Figure 3). Even more interesting is the comparison of the photometric properties among the three epochs of observations. Unlike the CMD location in EP2, the magnitudes derived for EP1 (F555W = 21.17 ± 0.06 and F336W = 23.04 ± 0.21) and for EP3 (F435W = 22.50 ± 0.03, F625W= 20.60 ± 0.03 and F658N = 20.27 ± 0.03) approximately locate the star onto the MS. Unfortunately, given the different instruments and filters, it is not possible to directly compare the magnitudes, but from both the visual inspection of images (see Figure 1) and the CMD locations with respect to the TO point, it turns out that during EP1 and EP3 the star was about 2–3 mag fainter than the TO and hence ∼2 mag fainter than in EP2. This likely indicates that the observations during EP1 and EP3 sampled the object in quiescence while EP2 data caught the star in an outburst state. In addition, during each epoch a magnitude modulation is present with an indication of a smaller amplitude in EP3 with respect to the variability detected during the EP2 outbursting state. In fact, the frame-to-frame magnitude scatter of the peculiar star during the outburst epoch (EP2) is 10σ–20σ larger than the scatter of normal stars in the same magnitude bin while this value decreases to $\sim 4\sigma$ in EP3.

In principle, for actively accreting LMXBs, Hα emission is expected from the accretion disk while the contribution from the heated companion star should be minimal or even absent. A visual inspection of EP2 images already suggests that this peculiar star also has Hα excess: in fact, in the F656N image (panel (e) in Figure 1) it is significantly brighter than its southern neighbor while these two objects show essentially the same magnitude in broadband filters (as the F390W, see panel (b) in Figure 1). In order to quantify this excess we used a photometric technique based on the comparison between the magnitudes obtained from broadband and Hα narrow filters (Cool et al. 1995). In particular, in this work we used a method commonly applied to star-forming regions (De Marchi et al. 2010) and

[5] It is important to note that, given the variability and an undersampled time coverage, the mean magnitudes (and hence the colors) derived here could not exactly correspond to the true average luminosities of the star over the entire variability period.

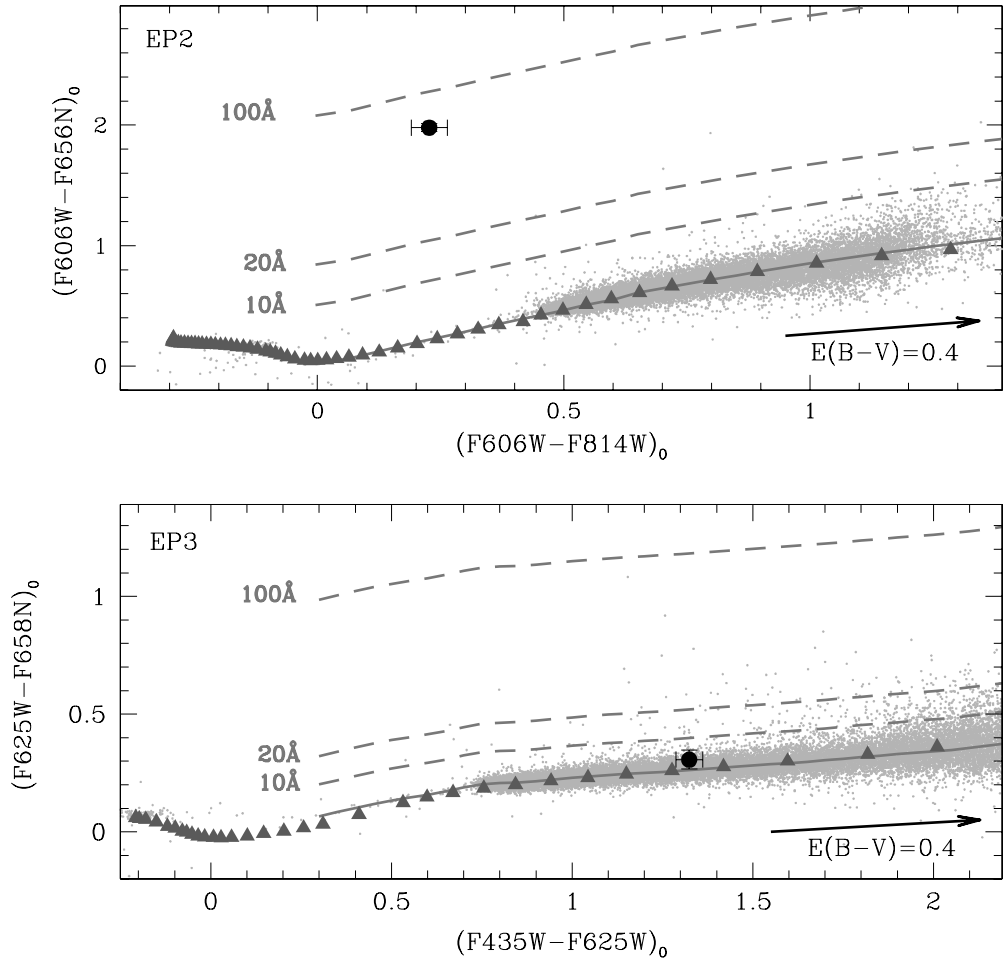

Figure 4. Reddening-corrected color–color diagrams for both EP2 and EP3. In each panel the solid line is the median color of stars (gray dots) with no Hα excess and hence the location of stars with $EW_{H\alpha} = 0$. It corresponds well to the location (gray triangles) predicted by atmospheric models (Bessell et al. 1998). Dashed lines show the expected position for stars with increasing levels of Hα emission, with the corresponding $EW_{H\alpha}$ labeled. The black dots mark the positions of the optical counterpart to IGR J1824−24525 in each epoch. During the outburst (upper panel) its Hα emission corresponds to $EW_{H\alpha} = 71.6^{+5.5}_{-5.1}$ Å, while in the quiescent state (lower panel) the star is located on the continuum reference line of stars with no Hα excess.

recently tested for the first time in the GC 47 Tucanae (Beccari et al. 2013; see also Beccari et al. 2013). First of all, we corrected all magnitudes for reddening by adopting $E(B - V) = 0.4$ (Harris 1996), then we selected the peculiar star in the (F606W-F656N)$_0$ versus (F606W-F814W)$_0$ color–color diagram. Note that this color combination samples the continuum of stars with no Hα emission for different spectral types through the (F606W-F814W)$_0$ color index well, and it provides a good estimate of the Hα emission through the (F606W-F656N)$_0$ color index, since the Hα line contribution to the F606W band is negligible. The Hα excess (ΔHα) can be evaluated from the distance between the (F606W-F656N)$_0$ color index of the considered star and an empirical line[6] representative of the continuum. In addition, the equivalent width (EW) of the Hα emission can be quantitatively estimated from ΔHα by applying Equation (4) in De Marchi et al. (2010): $EW_{H\alpha} = RW \times [1–10^{-0.4\times\Delta H\alpha}]$, where RW is the rectangular width of the filter (see Table 4 in De Marchi et al. 2010). With such a method, we estimated the Hα excess ($\Delta H\alpha = 1.98 \pm 0.03$; upper panel in Figure 4) and the EW of the Hα emission ($EW_{H\alpha} = 71.6^{+5.5}_{-5.1}$ Å, where the uncertainties take into account the errors in both colors) during the EP2 outburst state. By applying an analogous method to EP3 data, making use of a suitable combination of F435W, F625W, and F658N filters, we found that the star is located on the continuum reference line during its quiescent state (see the lower panel in Figure 4). Hence there is no indication of Hα emission in that epoch.

Finally, investigated the possible presence of UV emission by using the EP1 data set in filters F255W and F170W. No source was detected at the location of the peculiar star, most likely because the images are not deep enough to reach its faint magnitudes.

4. DISCUSSION AND CONCLUSIONS

Photometric analysis revealed the presence of a very peculiar star that underwent a strong luminosity increase and showed significant Hα excess in EP2. Even if this optical outburst occurred a few years before the *INTEGRAL* discovery, this evidence, combined with the positional coincidence with the ATCA variable source recently detected by Pavan et al. (ATel, 4981) and with the *Chandra* X-ray source 23 revealed by Becker et al.

[6] The reference line for the continuum has been determined from the median (F606W-F656N)$_0$ color as a function of (F606W-F814W)$_0$ for stars with combined photometric error smaller than 0.05 mag. As shown in Figure 4, this empirical relation agrees very well with the theoretical one obtained from atmospheric models (Bessell et al. 1998). We also emphasize that while M28 may be affected by mild differential reddening, the reddening vector is almost parallel to the empirical line tracing the continuum (see Figure 4). This means that even large fluctuations in the reddening of individual stars would not significantly affect the identification of objects with Hα excess (Beccari et al. 2010).

(2003) and firmly associated with IGR J1824−24525 by Homan & Pooley (2013), strongly suggests that we have identified the optical counterpart to IGR J1824−24525. Indeed several outbursts separated by a few years' delay are quite typical of LMXBs containing an NS (e.g., 4U 1608-52, Aquila X-1; Asai et al. 2012).

Unfortunately, the poor and irregular time coverage of our data prevented us from firmly determining the period of the magnitude modulation, which is expected to be correlated with the binary orbital motion. However, the non-regular shape of the light curve (likely due to an insufficient sampling of the orbital period) seems to suggest that the variability is occurring in a timescale a few times shorter than the duration of the observations (∼5–10 hr). This seems to be in agreement with the known properties of previously identified low-mass X-ray transients that have orbital periods in the range between 40 minutes and 4.3 hr (D'Avanzo et al. 2009) and even shorter in GCs (Homer et al. 2001; Zurek et al. 2009, and reference therein).

During the quiescent state the companion star is approximately located on the MS, ∼3 mag fainter than the TO, while during the outburst state it is ∼2 mag brighter and it is characterized by a bluer color. As known from the study of companions to MSPs and LMXBs, such an anomalous position is indicative of a perturbed state (see, e.g., Ferraro et al. 2001; Cocozza et al. 2008; Pallanca et al. 2010; Testa et al. 2012). In fact, tidal deformations, heating processes, and the presence of an accretion disk can significantly affect the magnitude and temperature of the star (E. Dalessandro et al., in preparation), altering its position in the CMDs. The main tool for discriminating between these effects is the determination of the light curve shape, but the available data sets prevent us from performing this study.

Finally, the presence of strong Hα emission (with $EW_{H\alpha} = 71.6^{+5.5}_{-5.1}$ Å) during the outburst phase suggests the presence of material accreting onto the NS. On the other hand, no Hα has been detected in quiescence, in agreement with the fact that when the accretion rate is slow, the disk is much weaker and the Hα absorption from the companion star dominates the spectrum.

Further optical studies are required to better constrain this system. First of all, a photometric follow-up with a suitable time sampling is needed to obtain accurate light curves and hence constrain the orbital parameters of the system. Also a spectroscopic analysis, which, given the high crowding and the relative faint magnitude, is possible only during a bright state, could help to characterize such a system and the possible presence of an accretion disk through the study of the radial velocity curve, the chemical abundance patterns, and UV emission lines. However, to properly derive the companion radial velocity curve, it is necessary to detect the spectral lines associated with the companion and to avoid those coming from the accretion disk.

This research is part of the project COSMIC-LAB (www.cosmic-lab.eu) funded by the European Research Council (under contract ERC-2010-AdG-267675). G.B. acknowledges the European Community's Seventh Framework Programme under grant agreement No. 229517.

Note added in proof. After the submission of this paper, XMM observations suggested that IGR J18245-2452 is the same source observed in the radio band as PSR J1824-2452I (Papitto et al. 2013).

REFERENCES

Asai, K., Matsuoka, M., Mihara, T., et al. 2012, PASJ, 64, 128
Bailyn, C. D. 1992, ApJ, 392, 519
Bailyn, C. D. 1995, ARA&A, 33, 133
Beccari, G., De Marchi, G., Panagia, N., & Pasquini, L. 2013, in IAU Symp. 290, Feeding Compact Objects: Accretion on All Scales, ed. C. Zhang, T. Belloni, M. Méndez, & S. Zhang (Paris: IAU), 187
Beccari, G., Spezzi, L., De Marchi, G., et al. 2010, ApJ, 720, 1108
Beccari, G., et al. 2013, MNRAS, submitted
Becker, W., Swartz, D. A., Pavlov, G. G., et al. 2003, ApJ, 594, 798
Bégin, S. 2006, M.Sc. thesis, Dept. of Physics and Astronomy, Univ. of British Columbia
Bellazzini, M., Pasquali, A., Federici, L., Ferraro, F. R., & Pecci, F. F. 1995, ApJ, 439, 687
Bessell, M. S., Castelli, F., & Plez, B. 1998, A&A, 333, 231
Bogdanov, S., van den Berg, M., Servillat, M., et al. 2011, ApJ, 730, 81
Chakrabarty, D., & Morgan, E. H. 1998, Natur, 394, 346
Clark, G. W. 1975, ApJL, 199, L143
Cocozza, G., Ferraro, F. R., Possenti, A., et al. 2008, ApJL, 679, L105
Cohn, H. N., Lugger, P. M., Bogdanov, S., et al. 2013, ATel, 5031
Cool, A. M., Grindlay, J. E., Cohn, H. N., Lugger, P. M., & Slavin, S. D. 1995, ApJ, 439, 695
D'Avanzo, P., Campana, S., Casares, J., et al. 2009, A&A, 508, 297
De Marchi, G., Panagia, N., & Romaniello, M. 2010, ApJ, 715, 1
Eckert, D., Del Santo, M., Bazzano, A., et al. 2013, ATel, 4925
Engel, M. C., Heinke, C. O., Sivakoff, G. R., Elshamouty, K. G., & Edmonds, P. D. 2012, ApJ, 747, 119
Ferraro, F. R., Beccari, G., Dalessandro, E., et al. 2009, Natur, 462, 1028
Ferraro, F. R., Fusi Pecci, F., & Bellazzini, M. 1995, A&A, 294, 80
Ferraro, F. R., Lanzoni, B., Dalessandro, E., et al. 2012, Natur, 492, 393
Ferraro, F. R., Possenti, A., D'Amico, N., & Sabbi, E. 2001, ApJL, 561, L93
Ferraro, F. R., Possenti, A., Sabbi, E., et al. 2003, ApJ, 595, 179
Fregeau, J. M. 2008, ApJL, 673, L25
Goodman, J., & Hut, P. 1989, Natur, 339, 40
Grindlay, J. E., Heinke, C., Edmonds, P. D., & Murray, S. S. 2001, Sci, 292, 2290
Harris, W. E. 1996, AJ, 112, 1487
Heinke, C. O., Bahramian, A., Wijnands, R., & Altamirano, D. 2013, ATel, 4927
Hills, J. G., & Day, C. A. 1976, ApL, 17, 87
Holtzman, J. A., Burrows, C. J., Casertano, S., et al. 1995, PASP, 107, 1065
Homan, J., & Pooley, D. 2013, ATel, 5045
Homer, L., Anderson, S. F., Margon, B., Deutsch, E. W., & Downes, R. A. 2001, ApJL, 550, L155
Hut, P., McMillan, S., Goodman, J., et al. 1992, PASP, 104, 981
Ivanova, N., Heinke, C. O., Rasio, F. A., Belczynski, K., & Fregeau, J. M. 2008, MNRAS, 386, 553
Linares, M. 2013, ATel, 4960
Lyne, A. G., Brinklow, A., Middleditch, J., Kulkarni, S. R., & Backer, D. C. 1987, Natur, 328, 399
Meylan, G., & Heggie, D. C. 1997, A&ARv, 8, 1
Pallanca, C., Dalessandro, E., Ferraro, F. R., et al. 2010, ApJ, 725, 1165
Pallanca, C., Dalessandro, E., Ferraro, R. F., Lanzoni, B., & Beccari, G. 2013, ATeL, 5003
Papitto, A., Ferrigno, C., Bozzo, E., et al. 2013, arXiv:1305.3884
Pavan, L., Wong, G., Wieringa, M. H., et al. 2013, ATel, 4981
Phinney, E. S. 1992, RSPTA, 341, 39
Pooley, D., Lewin, W. H. G., Anderson, S. F., et al. 2003, ApJL, 591, L131
Possenti, A., D'Amico, N., Manchester, R. N., et al. 2003, ApJ, 599, 475
Pryor, C., & Meylan, G. 1993, in ASP Conf. Ser. 50, Structure and Dynamics of Globular Clusters, ed. S. G. Djorgovski & G. Meylan (San Francisco, CA: ASP), 357
Romano, P., Barthelmy, S. D., & Burrows, D. N. 2013, ATel, 4929
Serino, M., Takagi, T., Negoro, H., et al. 2013, ATel, 4961
Sirianni, M., Jee, M. J., Benítez, N., et al. 2005, PASP, 117, 1049
Stetson, P. B. 1987, PASP, 99, 191
Stetson, P. B. 1994, PASP, 106, 250
Testa, V., di Salvo, T., D'Antona, F., et al. 2012, A&A, 547, A28
Verbunt, F., Bunk, W. H., Ritter, H., & Pfeffermann, E. 1997, A&A, 327, 602
White, N. E., Kaluzienski, J. L., & Swank, J. H. 1984, in AIP Conf. Proc. 115, High-Energy Transients in Astrophysics, ed. S. E. Woosley (Melville, NY: AIP), 31
Zurek, D. R., Knigge, C., Maccarone, T. J., Dieball, A., & Long, K. S. 2009, ApJ, 699, 1113